ELSEVIER

Biophysical Chemistry 116 (2005) 57–65

Biophysical Chemistry

http://www.elsevier.com/locate/biophyschem

Contribution of the multi-turn segment in the reversible thermal stability of hyperthermophile rubredoxin: NMR thermal chemical exchange analysis of sequence hybrids

David M. LeMaster, Jianzhong Tang, Diana I. Paredes, Griselda Hernández*

Wadsworth Center, New York State Department of Health and Department of Biomedical Sciences, University at Albany-SUNY, Empire State Plaza, Albany, New York 12201-0509, USA

Received 15 August 2004; received in revised form 27 January 2005; accepted 31 January 2005
Available online 26 February 2005

Abstract

Pyrococcus furiosus (*Pf*) rubredoxin is the most thermostable protein characterized to date. Reflecting the complications arising from irreversible denaturation of this protein, predictions of which structural regions confer differential thermal stability have utilized kinetic stability measurements, hydrogen exchange protection factors, long range hydrogen bond NMR spin couplings, and molecular dynamics simulations, and have primarily implicated the three-stranded β-sheet and the adjacent metal binding site. Herein, NMR chemical exchange experiments demonstrate reversible two-state unfolding at the thermal transition temperature (T_m) for hybrids of *Pf* and the mesophile *Clostridium pasteurianum* (*Cp*) rubredoxins which interchange residues 14–33, the so-called multi-turn segment. This complementary pair of hybrid rubredoxins exhibits largely additive incremental thermal stabilizations vs. the parental proteins. Both stabilization free energy measurements as well as incremental T_m values indicate that a minimum of 37% of the total differential thermal stability resides in this multi-turn segment. Such a proportionality between $\Delta\Delta G$ and incremental T_m values is predicted for hybrid pairs exhibiting thermodynamic additivity in which the differential stability is predominantly enthalpic.

Keywords: Rubredoxin; Reversible unfolding; Differential thermostability; NMR chemical exchange

1. Introduction

Archaeal phylogenetic families provide the vast majority of the hyperthermophilic organisms, including all of the most thermotolerant species, many with optimal growth temperatures above 100 °C. A number of proteins from the more modestly thermotolerant eubacteria *Thermotoga maritima* (optimal growth temperature 80 °C) have proven to be amenable to reversible unfolding studies [1–4]. Yet despite intense interest in understanding the structural basis of the thermal stability of the hyperthermophilic archaeal proteins, the homologous Sac7d and Sso7d from the *Sulfolobus* genus are the only such proteins for which mutational analysis combined with thermodynamic measurements has enabled assessment of the detailed stability contribution of particular structural elements [5,6]. This in turn reflects the fact that these Sac7d–Sso7d DNA binding proteins, with T_m values less than 100 °C, are among the few proteins from these organisms which have been shown to reversibly unfold under typical calorimetric conditions. The great majority of other studies of thermostability in proteins of hyperthermophilic archaea have monitored the kinetics of irreversible denaturation at elevated temperatures. Unfortunately, these measurements need not bear any clear relationship to the rate of reversible unfolding as illustrated for the protein under present study, rubredoxin, which at its T_m reversibly unfolds and refolds 10^7 times before the irreversible process occurs [7].

The rubredoxin from *Pyrococcus furiosus* (*Pf*) is the most thermostable protein characterized to date [7,8]. The

* Corresponding author. Tel.: +1 518 474 4673; fax: +1 518 473 2900.
E-mail address: griselda@wadsworth.org (G. Hernández).

0301-4622/$ - see front matter © 2005 Elsevier B.V. All rights reserved.
doi:10.1016/j.bpc.2005.01.010

15 most slowly exchanging amides of *Pf* rubredoxin are all clustered within the two cysteine-containing metal binding loops and the immediately adjacent proximal end of the three stranded β-sheet [8]. These are also the primary regions showing the largest differential hydrogen exchange rates in the comparison to the mesophile *Clostridium pasteurianum* (*Cp*) rubredoxin [9]. In the absence of known conditions for reversible unfolding, the effects of various mutational variants have been assessed using kinetic stability measurements in which the rate of loss of the optical signal of the tetracysteine-bound Fe^{3+} metal is monitored at elevated temperatures [10–12]. Kinetic stability measurements on a number of mutational variants have indicated that interactions between the β-sheet and core residues appear to be important in differential stabilization [11]. All of the long range hydrogen bond coupling constants observed in *Pf* rubredoxin lie within the metal site and proximal β-sheet region [13]. In addition to these various experimental studies implicating regions near the metal binding site and the proximal end of the β-sheet in the differential thermal stabilization of the rubredoxins, molecular dynamics calculations have also indicated hydrophobic packing between the β-strands in this role [14].

As characterized in the initial X-ray structure of *Cp* rubredoxin [15], a series of three 3_{10} turns makes up the majority of the sequence between residues 14 and 33 (*Cp* residue numbering used throughout) which form the surface opposite to that of the metal binding site (Fig. 1). Separation of this multi-turn region from the protein core initiates unfolding in molecular dynamics simulations [16]. Furthermore, the hydrogen exchange rates for the most slowly exchanging amides in this segment are quite similar for both *Cp* and *Pf* rubredoxins near room temperature, and are 10^2- to 10^3-fold less highly protected than those of the *Pf* core [9]. In addition, rubredoxin from the mesophilic *Desulfovibrio desulfuricans* exhibits a similar kinetic thermal stability to that of the *Cp* protein [17] despite lacking seven residues from the middle of the multi-turn segment [18]. These results are suggestive of a modest role of the multi-turn segment in the differential stabilization of the hyperthermophilic rubredoxin.

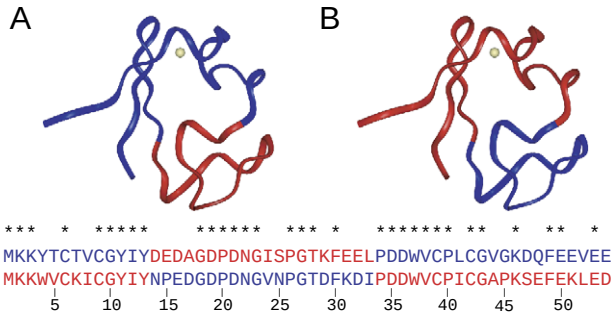

Fig. 1. Multi-turn segment swapped hybrids of *Pf* A2K and *Cp* rubredoxin. (A) *Cp* rubredoxin in which residues 14–33 have been substituted with the corresponding *Pf* sequence (red), denoted MT_{Pf}–*Cp* rubredoxin. (B) *Pf* A2K rubredoxin in which residues 14–33 have been substituted with the corresponding *Cp* sequence (blue), denoted MT_{Cp}–*Pf* A2K rubredoxin. This segment largely consists of three contiguous 3_{10} turns [34,35]. The metal atom is denoted in yellow. The conserved residues are marked by an asterisk.

On the other hand, for both *Pf* and *Cp* rubredoxins, the nine most protected amides between residues 14 and 32 exhibit a uniformity in their exchange rate constants as a function of temperature consistent with a subglobal collective conformational opening transition far below the global transition temperature [9]. Interestingly, a much weaker temperature dependence of this conformational opening equilibrium is observed for *Pf* rubredoxin. The resultant reduced $d\Delta G/dT$ dependence of this subglobal transition mimics the flattening of the global thermal stability curve that has commonly been invoked to explain the extended range of thermal stability observed among the hyperthermophile proteins.

Recently, we [7] reported that the reversible unfolding of both *Pf* and *Cp* rubredoxins can be observed via NMR chemical exchange dynamics measurements. This technique has been used to determine folding and unfolding rates near the thermal transition midpoint for a number of rapidly folding proteins [19–23]. Both *Pf* and *Cp* rubredoxins were found to (un)fold in a two-state transition at their respective thermal midpoints with a time constant of approximately 40 μs~10^7 times faster than the irreversible step monitored by loss of metal in the earlier kinetic thermal stability measurements. T_m values of 104 °C, 144 °C, and 137 °C, respectively, were observed for *Cp*, *Pf*, and an Ala 2-to-Lys variant of *Pf* rubredoxin (*Pf* A2K) possessing a *Cp*-like N-terminus. Although commonly utilized as a technique for measuring conformational dynamics, NMR thermal chemical exchange also offers a potentially sensitive means to directly measure the population of unfolded species well away from the thermal transition midpoint. A complementary pair of hybrid rubredoxins was designed in which the multi-turn segment is interchanged between the mesophile and hyperthermophile sequence. The differential thermal stabilities of these hybrid rubredoxins vs. the parental *Cp* and *Pf* A2K proteins were analyzed via NMR chemical exchange analysis.

2. Materials and methods

Escherichia coli codon-optimized sequences were used for design of the multi-turn sequence swapped hybrids. De novo gene construction utilized mutually priming long oligonucleotides [24]. The N-terminal half of the gene was synthesized from one oligonucleotide extending 36 bases from a *Nde*I restriction site at the initiator codon and a second oligonucleotide overlapping the first 15 bases and extending to the *Sma*I site encoding residues Gly 26 and Pro 27. The C-terminal half of the gene was similarly produced

from oligonucleotides covering the regions from the internal *Sma*I site to a *Bam*HI site immediately following the termination codon. Following primer extension, both products were digested with *Sma*I, ligated and the full length gene digested with *Nde*I and *Bam*HI and cloned into pET 3a.

Expression of the rubredoxin proteins was carried out in the BL21(DE3) system (Novagen), modified by introduction of a second plasmid which constitutively overproduces the methionine peptide deformylase to yield homogenous N-terminal processing [25]. The deuterated α-keto acids were prepared as previously described [26]. Samples of the Zn^{2+}-coordinated multi-turn sequence-swapped rubredoxins were expressed in protonated media containing either 100 mg/L α-ketoisovalerate (hyperthermophile multi-turn swapped *Cp* rubredoxin) or 50 mg/L α-ketobutyrate (mesophile multi-turn swapped *Pf* A2K rubredoxin). The defined medium and purification procedure were as previously described [9].

Protein samples for chemical exchange experiments were dialyzed into 100 mM sodium borate buffer in D_2O with a p*D** of 9, where p*D** is the uncorrected reading on a ^1H_2O-saturated probe. The samples were aliquoted into multiple NMR pressure tubes, and O_2 was purged by repeated freezing and evacuation. The tubes were then sealed under 35 psi of argon. Data collection and the temperature-dependent chemical shifts corrections were carried out as previously described [7]. The chemical shifts were normalized to the difference between the native state and model peptide values [27].

3. Results and discussion

3.1. NMR thermal chemical exchange

De novo gene construction was used to generate sequences in which residues 14–33 are interchanged between the parental *Cp* and *Pf* A2K proteins (Fig. 1). Use of the A2K variant helps circumvent complications of chemical heterogeneity in the N-terminal processing [25] as well as rendering these interactions analogous to those of the mesophile protein. As illustrated in this figure, the sequence between residues 14 and 33 not only spans the multi-turn segment, it is bounded on both the N- and C-terminal ends by a stretch of conserved residues, thus implying that any nonnative-like interactions which occur in the hybrid structures are likely to only arise from residues well separated along the sequence.

The NMR chemical exchange experiments involved the monitoring of the chemical shifts and linewidths of various ^1H resonances as a function of temperature. The upfield shifted methyl resonances are particularly informative in the rubredoxins. To facilitate both shift and linewidth analysis of the hyperthermophile multiturn-swapped *Cp* rubredoxin (MT_{Pf}–*Cp* rubredoxin), the leucine (and valine) methyl resonances were narrowed to a singlet by biosynthetic incorporation of 3-^{2}Hα-ketoisovalerate to eliminate the homonuclear coupling to the H^γ spin [26]. The analogous incorporation of 3-^{2}Hα-ketobutyrate served to narrow the isoleucine methyl resonances in the mesophile multiturn-swapped *Pf* A2K rubredoxin (MT_{Cp}–*Pf* A2K rubredoxin). NMR chemical exchange experiments were carried out on the diamagnetic Zn^{2+}-coordinated rubredoxin in 100 mM sodium borate in D_2O with a p*D** of 9 under 35 psi argon atmosphere to reduce potential oxidation reactions and suppress reflux at the elevated temperatures. Slightly basic conditions were chosen to help suppress protonation of the cysteine thiolates which occurs during loss of metal at lower pH values.

These experiments monitor the frequency shift and line broadening arising from the transfer of a nucleus between two (or more) environments at a rate comparable to the difference in resonance frequencies of these two states. As seen in the right-hand panel at 93 °C in Fig. 2, a sharp resonance near −1.35 ppm is observed for the $H^{\delta1}$ resonance of Leu 33 from the MT_{Pf}–*Cp* rubredoxin. As the temperature is raised, this resonance shifts and broadens

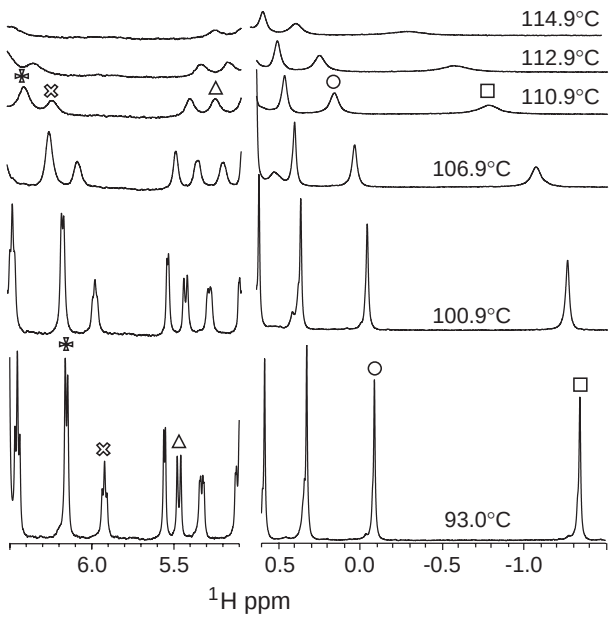

Fig. 2. NMR thermal chemical exchange titration for the Zn^{2+} form of rubredoxin from *Clostridium pasteurianum* containing the multi-turn segment (residues 14–33) from the *Pyrococcus furiosus* rubredoxin. The ^1H NMR spectral region between the aromatic and alpha random coil shift ranges (left) and the upfield region (right) is presented as a function of temperature. The amplitude of the upfield spectra is attenuated two-fold relative to those of the downfield region. The indicated resonances are: Leu 33 $H^{\delta1}$(□), Leu 33 $H^{\delta2}$(○), Phe 49 H^{α}(△), Trp 37 $H^{\zeta3}$(⊠), and Phe 30 H^{δ}(✠). Due to the nonlinear temperature dependence of the chemical shift for Thr 5 H^{α} (5.556 ppm at 93 °C) below the unfolding transition, accurate population estimates were not obtained. The leucine (and valine) methyl resonances were narrowed to a singlet by biosynthetic incorporation of 3-^{2}Hα-ketoisovalerate to eliminate the homonuclear coupling to the H^γ spin [26].

as expected for a resonance arising from a dynamic interchange of folded and unfolded conformations which are exchanging in a microsecond–millisecond timeframe. Other resonances undergo similar changes both in the upfield methyl region as well as in the spectral region between the random coil aromatic and alpha chemical shifts (left-hand panel). By focusing on resonances which in the native state are strongly shifted from their reference random coil values, these measurements of reversible folding under equilibrium conditions can be carried out in the presence of a substantial degree of irreversible denaturation. As such strongly shifted resonances are not expected (or observed) in the irreversibly denatured component of the sample, the resonances in these spectral regions arise only from a dynamical averaging of the reversibly unfolded and folded states. Although the irreversible step results in loss of intensity for the signals arising from the reversible folding process, the chemical shifts and linewidths of these resonances are unaffected [7].

3.2. Population analysis of the folding transition

At higher temperatures, the irreversible denaturation process precludes the direct observation of the resonances arising from the reversibly unfolded state. Model peptide shifts [27] were used to approximate the chemical shifts in the reversibly unfolded state. Focusing on resonances which are strongly shifted in the native state serves to minimize the errors in T_m estimation arising from inaccuracies in the model peptide referencing. For these monitored resonances, a linear temperature dependence of the chemical shift was directly verified by analysis of spectra collected below the onset of the unfolding transition. The fraction of unfolded protein can then be estimated by normalizing the difference between the observed ^{1}H shift vs. the model peptide value to the difference between the native state ^{1}H shift and that model peptide value (Fig. 3).

The close fit among the data for all five resonances is consistent with a lack of significant local structure in the unfolded state which if present would likely perturb the resonances away from the model peptide values. Over half of the transition is explicitly monitored utilizing sidechain and backbone resonances located within the aromatic cluster in the hydrophobic core. As discussed below, the enthalpy of reversible unfolding for the hybrid rubredoxins is comparable to those determined for parental proteins [7] which correspond well with the values previously estimated from irreversible denaturation as monitored by circular dichroism, fluorescence, and absorption [28]. The arguments that these data monitor the global unfolding transition, previously discussed for the parental proteins [7], hold equally well for these hybrid rubredoxins.

As demonstrated previously [7] and in the data of Fig. 3, the temperature dependence of the unfolded populations for both parental and hybrid rubredoxins conforms

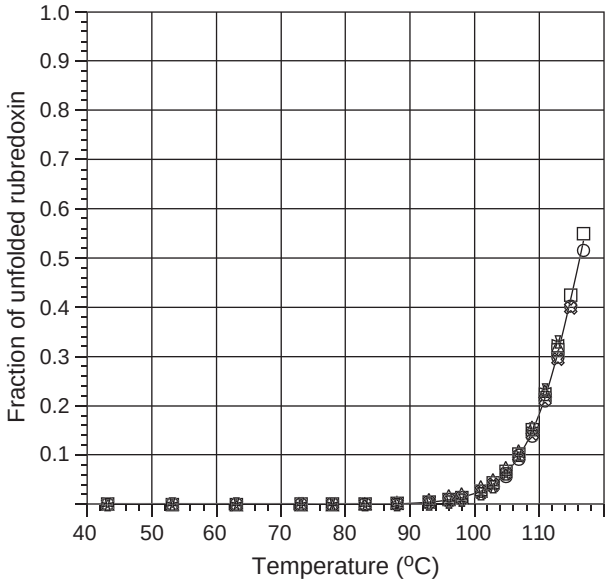

Fig. 3. Population analysis for the thermal transition of the Zn^{2+} form of rubredoxin from *Clostridium pasteurianum* containing the multi-turn segment (residues 14–33) from the *Pyrococcus furiosus* rubredoxin. Normalized chemical shift migrations were calculated from the data of Fig. 2 with the individual resonances similarly indicated. From the NMR spectra collected more than 30° below the T_m, the chemical shift differences between the monitored resonance and the highly exposed N-terminal Met methyl resonance were used to determine a linear temperature dependence of the relative native state chemical shifts. The Met methyl resonance exhibited minimal temperature variation with respect to external d_4-3-(trimethylsilyl)propionate. The observed chemical shift migration is normalized to the difference between the native state and model peptide chemical shifts [27]. Optimal fit to the two-state Gibbs–Helmholtz equation is given with ΔC_p set to 0.5 kcal/mol deg.

quite closely to the modified Gibbs–Helmholtz equation derived by assuming a temperature-independent heat capacity:

$$\Delta G(T) = \Delta H_{T\mathrm{m}}(1 - T/T_m) + \Delta C_p[(T - T_m) - T\ln(T/T_m)] \quad (1)$$

Such unfolding behavior is indicative of a reversible two-state transition. In particular, *Pf* A2K was previously determined to have a thermal transition temperature of 137.0 (±0.4) °C with an estimated unfolding enthalpy of 79.8 (±2.5) kcal/mol which, given that $\Delta S_{T_m} = \Delta H_{T_m}/T_m$, implies a transition entropy of 0.195 kcal/mol deg. Table 1 lists the corresponding enthalpy and entropy values at the thermal transition midpoint for each rubredoxin. These values were derived from the two state analysis by assuming a heat capacity value of 0.5 kcal/mol deg consistent with the known correlation between ΔC_p and protein molecular weight [29]. Variation of the assumed ΔC_p value from 0 to 1.0 kcal/mol deg altered the estimated enthalpy less than the rmsd among the enthalpy values estimated from the individual resonances (e.g., 2.5 kcal/mol for *Pf* A2K). In addition, this variation of the assumed ΔC_p value altered the derived T_m values by only 0.1°.

Table 1
Thermodynamic parameters of rubredoxin unfolding equilibria

	T_m	$T_m - T_m$ (*Cp*)	ΔH_{T_m}	ΔH_{T_m}(*Pf* A2K)[a]	ΔS_{T_m}	ΔS_{T_m}(*Pf* A2K)[a]
Pf A2K	137.0 (0.4)	32.7	79.8 (2.5)	–	0.195	–
MT_{Cp}–*Pf* A2K	119.5 (1.6)	15.2	51.8 (2.5)	71.0	0.132	0.173
MT_{Pf}–*Cp*	116.3 (0.4)	12.0	71.7 (2.3)	69.5	0.184	0.169
Cp	104.3 (0.3)	–	62.3 (3.0)	63.5	0.160	0.153

[a] Thermodynamic parameters of *Pf* A2K rubredoxin derived at the T_m values for the other rubredoxins by assuming a ΔC_p value of 0.5 kcal/mol deg.

Given the basic thermodynamic relationships:

$$\Delta S = \Delta S^o + \Delta C_p \ln(T/T^o) \quad (2)$$

$$\Delta H = \Delta H^o + \Delta C_p (T - T^o) \quad (3)$$

and applying the assumed ΔC_p value of 0.5 kcal/mol deg, the enthalpy and entropy of *Pf* A2K rubredoxin were calculated at the thermal transition temperatures of the other rubredoxins (Table 1). These predicted enthalpy and entropy values for *Pf* A2K rubredoxin agree fairly closely with those of the parental *Cp* as well as for the MT_{Pf}–*Cp* hybrid. On the other hand, the observed ΔH and ΔS values for the MT_{Cp}–*Pf* hybrid at its thermal transition midpoint differ markedly from those predicted for *Pf* A2K rubredoxin under these conditions.

As noted, the NMR thermal chemical exchange experiment provides direct population estimates independent of any thermodynamic modeling beyond the assumption of a two-state transition. Given total resonance shift migration ranges which can exceed 1000 Hz at an 11.7 T magnetic field strength and peak positions determined to less than 1 Hz, the precision of such population estimates is quite high. On the other hand, the accuracy of the population estimate from any single resonance is potentially open to challenge. However, the five monitored resonances of the MT_{Pf}–*Cp* rubredoxin represent differing positions within the protein core, and they migrate by differing amounts and in opposite frequency directions. The close correspondence for the population estimates obtained from each of these resonances argues for the robustness of the analysis.

As the T_m values for the two multi-turn hybrid proteins are similar, determination of the reversibly unfolded fraction for each protein at a given temperature can be used to directly determine their relative thermodynamic stabilities. At 117.8 °C the unfolded population values of 0.430 and 0.597 for MT_{Cp}–*Pf* rubredoxin and MT_{Pf}–*Cp* rubredoxin, respectively, yield a differential thermodynamic stability of 0.52 kcal/mol. The variation in the population estimates obtained for the individual resonances, weighted by the magnitude of the frequency migration observed for that resonance, yields an uncertainty estimate of 0.06 kcal/mol. In a similar fashion, the differential free energy of stabilization was determined between each parental and hybrid rubredoxin (Fig. 4).

The temperature dependence of the free energy of stability curve $\delta\Delta G/\delta T$ is equal to the negative of the entropy of unfolding $-\Delta S$. The data of Fig. 4 represent a true thermodynamic cycle only if differential entropy among the rubredoxins $\Delta\Delta S$=0, or, equivalently, if the free energy differences between the proteins in this temperature range, are determined by their differences in enthalpy. As indicated in the upper triangle of this figure, the free energy difference between *Pf* A2K rubredoxin and the MT_{Pf}–*Cp* hybrid is predicted to be the same when measured directly or via the MT_{Cp}–*Pf* hybrid. This primarily reflects the fact that the two major free energy transitions are monitoring the temperature dependence of the same protein, *Pf* A2K rubredoxin. In contrast, the data in the lower triangle markedly deviate from such behavior as the free difference determined for the direct parental *Cp* to MT_{Cp}–*Pf* hybrid transition is approximately 0.6 kcal/mol less than that estimated via the MT_{Pf}–*Cp* hybrid. The fact that the $\Delta\Delta G$ value for the *Cp* to MT_{Cp}–*Pf* hybrid transition is smaller than that for the complementary hybrid despite the higher T_m of the MT_{Cp}–*Pf* hybrid indicates a smaller entropy of unfolding in this temperature range. The data of Table 1 indicate that at its thermal transition midpoint, the entropy for the MT_{Cp}–*Pf* hybrid is approximately 0.05 kcal/mol deg less than that of

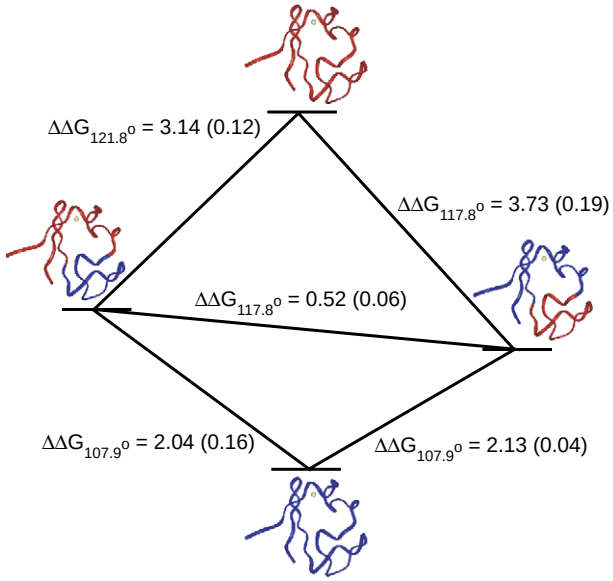

Fig. 4. Nominal thermodynamic cycle for the parental *Cp* and *Pf* A2K rubredoxins and their multi-turn swapped hybrids. Temperatures were identified at which the population of unfolded species could be simultaneously determined for two or more of the rubredoxins. The differential free energies of stabilization were determined (kcal/mol) with the rmsd, indicated in parentheses, being derived from the values predicted from each monitored resonance.

the complementary hybrid. Over the 12–15° temperature interval to the T_m of the parental *Cp* protein, this entropy difference predicts a 0.6–0.7 kcal/mol difference in free energy.

The direct population measurements as well as the T_m and ΔH_{T_m} values on which the foregoing analysis is based are largely independent of an assumed ΔC_p value. On the other hand, these data provide a basis to assess the consistency of an assumed ΔC_p value in the neighborhood of 0.5 kcal/mol deg. The ΔH and ΔS values derived for the parental *Pf* A2K rubredoxin at the T_m of MT_{Pf}–*Cp* hybrid are similar to those of that hybrid. As a result, the $\Delta\Delta G$ of *Pf* A2K rubredoxin at the thermal transition midpoint of *Cp* rubredoxin can be estimated to be 5.8 kcal/mol from the free energy differences of the MT_{Pf}–*Cp* hybrid with respect to each parental protein. Additional support for this free energy estimate comes from an independent pair of complementary hybrids for which each branch of the corresponding nominal thermodynamic cycle yields a similar 5.8 kcal/mol differential stability for the parental *Cp* and *Pf* A2K proteins (LeMaster and Hernández, in preparation). Application of the modified Gibbs–Helmholtz equation to the observed *Pf* A2K rubredoxin thermodynamic parameters by assuming this 5.8 kcal/mol differential stability yields a ΔC_p value for this protein of 0.43 (±0.15) kcal/mol deg.

3.3. Relationship between differential free energy of stability and incremental T_m values

The fact that the MT_{Pf}–*Cp* hybrid is 2.13 kcal/mol more thermostable than the parental *Cp* rubredoxin indicates that the hyperthermophile multi-turn sequence must provide at least 37% (2.13/5.8) of the total differential stability of the parental proteins. Strikingly, the difference in the T_m value of this hybrid vs. those of the parental rubredoxins also yields a lower bound estimate of 37% (12.0°/32.7°) for the contribution of the hyperthermophile multi-turn sequence to the thermostabilization. An upper bound to this estimate can be similarly obtained by considering the complementary transition between *Pf* A2K and the MT_{Cp}–*Pf* hybrid in which the multi-turn sequence is interchanged on the hyperthermophile protein core. At most, this segment can account for 54% (3.14/5.8) of the total differential free energy of stabilization. Once again, the maximal contribution of the differential thermostabilization based on the T_m values yields the equivalent result of 54% (17.5°/32.7°).

As the correlation between increased free energy of stabilization and increased T_m values is commonly regarded as qualitative at best, it is worth considering what factors can account for their close correspondence in the present case. Making use of the fact that the slope of the thermal stability curve is $-\Delta S$ and that $\Delta S = \Delta H/T$ at the thermal transition midpoint, Becktel and Schellman [30] have observed that, if the entropy of unfolding is unaffected by a weakly perturbing mutation, then $\Delta\Delta G$ for the parental vs. mutant protein can be estimated as $\Delta T_m \Delta S_{T_m}$. This argument can be extended for the case of a complementary hybrid pair exhibiting thermodynamic additivity by replacing the assumption of a temperature-independent entropy of unfolding with the assumption of a temperature-independent heat capacity.

Consider the case in which the differential free energies of stabilization among the parental (P1 and P2) and hybrid (H1 and H2) proteins arise from purely enthalpic contributions. In this case, all species have the same entropy dependence as a function of temperature. Hence to determine the free energy of the thermophile parental protein (P1) at the thermal transition temperature of the mesophile parent (P2), the entropy expression of Eq. (2) is substituted into the modified Gibbs–Helmholtz equation (Eq. (1)) to yield:

$$\begin{aligned}\Delta G_{T\mathrm{m(P2)}}(\mathrm{P1}) = {} & T_{\mathrm{m(P1)}}\left[\Delta S_{T\mathrm{m(P2)}} + \Delta C_p \ln\left(T_{\mathrm{m(P1)}}/T_{\mathrm{m(P2)}}\right)\right] \\ & \times \left(1 - T_{\mathrm{m(P2)}}/T_{\mathrm{m(P1)}}\right) + \Delta C_p\left[\left(T_{\mathrm{m(P2)}}\right.\right. \\ & \left.\left. - T_{\mathrm{m(P1)}}\right) - T_{\mathrm{m(P2)}} \ln\left(T_{\mathrm{m(P2)}}/T_{\mathrm{m(P1)}}\right)\right] \quad (4)\end{aligned}$$

The analogous equations apply for the thermodynamic stability of the hybrids at the T_m of the mesophile parent protein with the same entropy dependence assumed. Thermodynamic additivity implies that:

$$\Delta G_{T\mathrm{m(P2)}}(\mathrm{P1}) = \Delta G_{T\mathrm{m(P2)}}(\mathrm{H1}) + \Delta G_{T\mathrm{m(P2)}}(\mathrm{H2}) \quad (5)$$

Combining Eqs. (4) and (5) for P1, H1, and H2 and rearranging yields:

$$\begin{aligned}&\left[\left[\left(T_{\mathrm{m(P1)}} + T_{\mathrm{m(P2)}}\right] - \left[T_{\mathrm{m(H1)}} + T_{\mathrm{m(H2)}}\right]\right]\right. \\ &\quad = \left[\Delta C_p/\left(\Delta C_p - \Delta S_{T\mathrm{m(P2)}}\right)\right]\left[T_{\mathrm{m(P1)}} \ln\left(T_{\mathrm{m(P1)}}/T_{\mathrm{m(P2)}}\right)\right. \\ &\qquad \left.\left. - T_{\mathrm{m(H1)}} \ln\left(T_{\mathrm{m(H1)}}/T_{\mathrm{m(P2)}}\right) - T_{\mathrm{m(H2)}} \ln\left(T_{\mathrm{m(H2)}}/T_{\mathrm{m(P2)}}\right)\right]\right] \quad (6)\end{aligned}$$

The maximum deviation between the sum of the parental and sum of hybrid T_m values occurs when both hybrid T_m values are equal approximately midway in between the parental T_m values. Applying the thermodynamic parameters for the parental rubredoxins yields a sum of the hybrid rubredoxin T_m values which exceeds that of the parental proteins by, at most, 1.6°. Furthermore, as ΔC_p is always greater than ΔS, the right-hand side of Eq. (6) changes sign before the left-hand side reaches zero, indicative of the fact that for enthalpy-dominated differential free energies of unfolding for thermodynamically additive hybrids, the sum of the hybrid T_m values always exceeds that of the parental proteins.

Clearly, the complementary multi-turn hybrid rubredoxin system does not fully satisfy the conditions of strict thermodynamic additivity or enthalpy-dominated differential free energies of stabilization. With respect to the thermal transition midpoint of the parental *Cp* rubredoxin, the T_m increments of these two hybrids add up to 83% of the differential for the *Pf* A2K protein. Furthermore, partic-

ularly for the transition relating the MT_{Cp}–*Pf* hybrid to the parental *Cp* protein, the assumption of equivalent entropy functions appears to not be justified. On the other hand, that transition does not directly contribute to the $\Delta\Delta G$ vs. incremental T_m correlations discussed above. In contrast, the ΔC_p-based estimates of the temperature dependence of the *Pf* A2K enthalpy and entropy (Table 1) suggest a reasonable correlation with those of *Cp* and the MT_{Pf}–*Cp* hybrid. Hence, the direct correlation of $\Delta\Delta G$ with differential T_m values predicted for the enthalpy-dominated $\Delta\Delta G$ of thermodynamically additive hybrids appears to be sufficiently robust to extend to cases which moderately deviate from the assumed conditions.

3.4. Spatial distribution of differential thermal stabilization

The markedly lower ΔH_{T_m} and ΔS_{T_m} values of the MT_{Cp}–*Pf* hybrid relative to those of the other rubredoxins in this study support the interpretation that interactions in this hybrid are likely to be the major cause of the lack of complete thermodynamic additivity observed for the complementary multi-turn hybrid system. If in contrast the MT_{Pf}–*Cp* hybrid exhibits behavior more consistent with thermodynamic additivity, it is worth considering how that behavior might be achieved. Conceptually, the most straightforward approach to potentially achieving thermodynamic additivity in a complementary hybrid system is to have every energetically significant interaction present in the hybrid structure correspond directly to the analogous interaction in one of the two parental proteins. The interactions in the complementary hybrid would likewise correspond to the complementary set of interactions present in the two parental proteins. Violation of this condition would arise from interactions present in the hybrid but absent in both of the two parental proteins or present in one parent but absent in both hybrid proteins.

Fig. 5 illustrates a CPK model of *Cp* rubredoxin in which the residues involved in the multi-turn segment have been removed. Colored in green are the residues that are conserved between *Cp* and *Pf* rubredoxins which exhibit increased surface accessibility when the multi-turn segment is removed. The only nonconserved residue in contact with the multi-turn segment is Tyr 4 (marked in red) which interacts along the face of its phenyl ring in a base stacking interaction with the phenyl ring of the conserved Phe 30 residue. Its phenolic OH group extends out into solvent. In *Pf* rubredoxin, Trp 4 adopts the analogous base stacking interaction with Phe 30. When the hyperthermophile multi-turn segment is attached to the mesophile protein core, the Glu 15 sidechain is introduced. In *Pf* rubredoxin the Glu 15 sidechain interacts with the indole H^N through a moderately long (2.2 Å) hydrogen bond. If a simple conception of pairwise additivity is to be satisfied, an energetically equivalent interaction must be formed in the MT_{Pf}–*Cp* hybrid.

This expectation is supported by the recent structural analysis of *Pf* rubredoxin in which a Trp 4→Tyr 4 mutation was introduced along with *Cp*-like substitutions of Ile 24→Val 24 and Leu 33→Ile 33 in the multi-turn segment [31]. Minimal change was observed around the sidechains of 24 and 33. The sidechain of Glu 15 maintains its orientation, and a water molecule provides a bridging hydrogen bond between its carboxylate and the Tyr 4 phenolic OH.

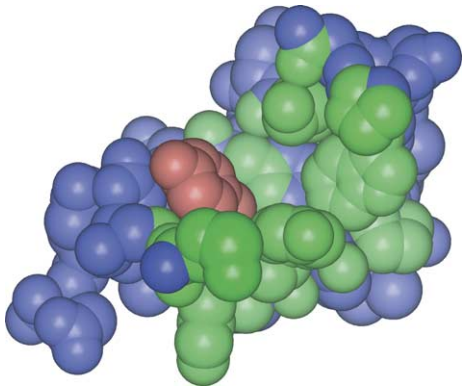

Fig. 5. Evolutionary conservation in the rubredoxin core along the interface with the multi-turn segment. A CPK model of *Cp* rubredoxin (5RXN) [34] in which residues 14–33 have been removed. Atoms denoted in blue undergo no change in static accessible surface area [36] (probe radius 1.4 Å) when the multi-turn segment is removed. Sidechains in the interface which are conserved between the mesophile and hyperthermophile rubredoxins are highlighted in green, while Tyr 4, denoted in red, is substituted for Trp in the *Pf* protein.

4. Conclusions

The rubredoxin from *Pf* has generated considerable interest due to its manifesting the highest degree of protein thermostabilization known. Unfortunately, the initial inability to monitor the reversible folding transition necessitated indirect estimates of global stability. The NMR thermal chemical exchange technique allows for unfolding equilibria to be measured in the thermal transition region, thus circumventing problems arising from indirect estimates of thermodynamic stability [8]. In the favorable circumstances presented by the rubredoxin data, these chemical exchange experiments provide for accurate measurement of unfolded populations at levels as low as 1%. This in turn has enabled direct determination of the relative stability equilibria for rubredoxin variants with T_m values differing by 20°.

Despite the technical complications introduced by its elevated thermal unfolding temperature, *Pf* rubredoxin presents a well behaved model system for the detailed analysis of the structural basis of differential thermal stabilization. Its rapid two-state thermal global unfolding occurs at a rate consistent with that predicted from contact order analysis [7,32]. Its tolerance of high pH has facilitated analysis of rapid hydrogen exchange by magnetization transfer techniques [9,33]. Systematic mutagenesis studies,

combined with NMR thermal chemical exchange measurements, offer a promising path to understanding the degree to which differential thermal stabilization can be structurally localized and to analyzing how these structural variants affect the conformational dynamics of the protein. This study demonstrates that a minimum of 37% of the differential thermal stability of *Pf* A2K rubredoxin vs. its mesophile *Cp* homolog resides in the multi-turn segment. This substantial differential stabilization arises from this segment despite the fact that this region is known to undergo a collective opening transition with a similar probability for both the mesophile and hyperthermophile rubredoxins near room temperature roughly 100° below the thermal transition temperature near neutral pH.

It is shown that for hybrid pairs which exhibit thermodynamic additivity with respect to the parental proteins and for which the differential stability is predominantly enthalpic, the differential increments in T_m are near perfectly proportionate to the differential thermodynamic stabilities. Although neither of these conditions is completely satisfied for the multi-turn swapped rubredoxin hybrid system, the observed proportionality between $\Delta\Delta G$ and incremental T_m values suggests that this correlation is yet more robust.

Acknowledgments

We acknowledge the use of the Wadsworth Center NMR facility and the technical assistance of Lynn McNaughton as well as the Wadsworth Center Molecular Genetics Core. This work was supported in part by NIH grant GM 64736 (G.H.).

References

[1] D. Wassenberg, C. Welker, R. Jaenicke, Thermodynamics of the unfolding of the cold-shock protein from *Thermotoga maritima*, J. Mol. Biol. 289 (1999) 187–193.

[2] T. Dams, R. Jaenicke, Stability and folding of dihydrofolate reductase from the hyperthermophilic bacterium *Thermotoga maritima*, Biochemistry 38 (1999) 9169–9178.

[3] W.A. Deutschman, F.W. Dahlquist, Thermodynamic basis for the increased thermostability of CheY from the hyperthermophile *Thermotoga maritima*, Biochemistry 40 (2001) 13107–13113.

[4] J.H.G. Lebbink, V. Consalvi, R. Chiaraluce, K.D. Berndt, R. Ladenstein, Structural and thermodynamic studies on a salt-bridge triad in the NADP-binding domain of glutamate dehydrogenase from *Thermotoga maritima*: cooperativity and electrostatic contribution to stability, Biochemistry 41 (2002) 15524–15535.

[5] E. Mombelli, M. Afshar, P. Fusi, M. Mariani, P. Tortora, J.P. Connelly, R. Lange, The role of phenylalanine 31 in maintaining the conformational stability of ribonuclease P2 from *Sulfolobus solfataricus* under extreme conditions of temperature and pressure, Biochemistry 36 (1997) 8733–8742.

[6] A.T. Clark, B.S. McCrary, S.P. Edmondson, J.W. Shriver, Thermodynamics of core hydrophobicity and packing in the hyperthermophile protein Sac7d and Sso7d, Biochemistry 43 (2004) 2840–2853.

[7] D.M. LeMaster, J. Tang, G. Hernández, Absence of kinetic thermal stabilization in a hyperthermophile rubredoxin indicated by 40 microsecond folding in the presence of irreversible denaturation, Proteins 57 (2004) 118–127.

[8] R. Hiller, Z.H. Zhou, M.W.W. Adams, S.W. Englander, Stability and dynamics in a hyperthermophilic protein with melting temperature close to 200 degrees C, Proc. Natl. Acad. Sci. U. S. A. 94 (1997) 11329–11332.

[9] G. Hernández, D.M. LeMaster, Reduced temperature dependence of collective conformational opening in a hyperthermophile rubredoxin, Biochemistry 40 (2001) 14384–14391.

[10] S. Cavagnero, Z.H. Zhou, M.W.W. Adams, S.I. Chan, Response of rubredoxin from *Pyrococcus furiosus* to environmental changes: implications for the origin of hyperthermostability, Biochemistry 34 (1995) 9865–9873.

[11] M.K. Eidsness, K.A. Richie, A.E. Burden, D.M. Kurtz, R.A. Scott, Dissecting contributions to the thermostability of *Pyrococcus furiosus* rubredoxin: beta-sheet chimeras, Biochemistry 36 (1997) 10406–10413.

[12] S. Cavagnero, Z.H. Zhou, M.W.W. Adams, S.I. Chan, Unfolding mechanism of rubredoxin from *Pyrococcus furiosus*, Biochemistry 37 (1998) 3377–3385.

[13] C.M. Bougault, M.K. Eidsness, J.H. Prestegard, Hydrogen bonds in rubredoxins from mesophilic and hyperthermophilic organisms, Biochemistry 42 (2003) 4357–4372.

[14] D.H. Jung, N.S. Kang, M.S. Jhon, Site-directed mutation study on hyperthermostability of rubredoxin from *Pyrococcus furiosus* using molecular dynamics simulations in solution, J. Phys. Chem., A 101 (1997) 466–471.

[15] K.D. Watenpaugh, L.C. Sieker, L.H. Jensen, The structure of rubredoxin at 1.2 Å resolution, J. Mol. Biol. 131 (1979) 509–522.

[16] T. Lazaridis, I. Lee, M. Karplus, Dynamics and unfolding pathways of a hyperthermophilic and a mesophilic rubredoxin, Protein Sci. 6 (1997) 2589–2605.

[17] P. Lamosa, A. Burke, R. Peist, R. Huber, M.Y. Liu, G. Silva, C. Rodrigues-Pousada, J. LeGall, C. Maycock, H. Santos, Thermostabilization of proteins by diglycerol phosphate, a new compatible solute from the hyperthermophile *Archaeoglobus fulgidus*, Appl. Environ. Microbiol. 66 (2000) 1974–1979.

[18] L.C. Sieker, R.E. Stenkamp, L.H. Jensen, B. Prickril, J. LeGall, Structure of rubredoxin from the bacterium *Desulfovibrio desulfuricans*, FEBS Lett. 208 (1986) 73–76.

[19] G.S. Huang, T.G. Oas, Submillisecond folding of monomeric λ repressor, Proc. Natl. Acad. Sci. U. S. A. 92 (1995) 6878–6882.

[20] R.E. Burton, G.S. Huang, M.A. Daughterty, P.W. Fullbright, T.G. Oas, Microsecond protein folding through a compact transition state, J. Mol. Biol. 263 (1996) 311–322.

[21] J.K. Myers, T.G. Oas, Preorganized secondary structure as an important determinant of fast protein folding, Nat. Struct. Biol. 8 (2001) 552–558.

[22] J.K. Myers, T.G. Oas, Mechanisms of fast protein folding, Annu. Rev. Biochem. 71 (2002) 783–815.

[23] U. Mayor, N.R. Guydosh, C.M. Johnson, J.G. Grossmann, S. Sato, G.S. Jas, S.M.V. Freund, D.O.V. Alonso, V. Daggett, A.R. Fersht, The complete folding pathway of a protein from nanoseconds to microseconds, Nature 421 (2003) 863–867.

[24] D.D. Moore, in: V.B. Chandra (Ed.), Current Protocols in Molecular Biology, vol. 1, John Wiley & Sons, New York, 1994, pp. 8.2.8–8.2.13.

[25] J. Tang, G. Hernández, D.M. LeMaster, Increased peptide deformylase activity for the *N*-formylmethionine processing of proteins overexpressed in *Escherichia coli*: application to homogeneous rubredoxin production, Protein Expr. Purif. 36 (2004) 100–105.

[26] N.K. Goto, K.H. Gardner, G.A. Mueller, R.C. Willis, L.E. Kay, A robust and cost-effective method for the production of Val, Leu, Ile(δ1) methyl-protonated ^{15}N, ^{13}C, ^{2}H labeled proteins, J. Biomol. NMR 13 (1999) 369–374.

[27] M.R. Arnold, W. Kremer, H.D. Lüdemann, H.R. Kalbitzer, ^{1}H-NMR parameters of common amino acid residues measured in aqueous solutions of the linear tetrapeptides Gly-Gly-X-Ala at

pressures between 0.1 and 200 MPa, Biophys. Chemist. 96 (2002) 129–140.
[28] S. Cavagnero, D.A. Debe, Z.H. Zhou, M.W.W. Adams, S.I. Chan, Kinetic role of electrostatic interactions in the unfolding of hyperthermophilic and mesophilic rubredoxins, Biochemistry 37 (1998) 3369–3376.
[29] J.K. Myers, C.N. Pace, J.M. Scholtz, Denaturant m values and heat-capacity changes: relation to changes in accessible surface areas of protein folding, Protein Sci. 4 (1995) 2138–2148.
[30] W.J. Becktel, J.A. Schellman, Protein stability curves, Biopolymers 26 (1987) 1859–1877.
[31] T. Chatake, K. Kurihara, I. Tanaka, I. Tsyba, R. Bau, F.E. Jenney, M.W.W. Adams, N. Niimura, A neutron crystallographic analysis of a rubredoxin mutant at 1.6 Å resolution, Acta Crystallogr., D Biol. Crystallogr. 60 (2004) 1364–1373.
[32] K.W. Plaxco, K.T. Simons, D. Baker, Contact order, transition state placement and the refolding rates of single domain proteins, J. Mol. Biol. 277 (1998) 985–994.
[33] G. Hernández, F.E. Jenney, M.W.W. Adams, D.M. LeMaster, Millisecond time scale conformational flexibility in a hyperthermophile protein at ambient temperature, Proc. Natl. Acad. Sci. U. S. A. 97 (2000) 3166–3170.
[34] K.D. Watenpaugh, L.C. Sieker, L.H. Jensen, Crystallographic refinement of rubredoxin at 1.2 Å resolution, J. Mol. Biol. 138 (1980) 615–633.
[35] R. Bau, D.C. Rees, D.M. Kurtz, R.A. Scott, H.S. Huang, M.W.W. Adams, M.K. Eidsness, Crystal-structure of rubredoxin from *Pyrococcus furiosus* at 0.95 angstrom resolution, and the structures of N-terminal methionine and formylmethionine variants of *Pf* Rd. Contributions of N-terminal interactions to thermostability, J. Biol. Inorg. Chem. 3 (1998) 484–493.
[36] B. Lee, F.M. Richards, The interpretation of protein structures: estimation of static accessibility, J. Mol. Biol. 55 (1971) 379–400.